Co-published by
Institute of Fluid-Flow Machinery
Polish Academy of Sciences
Committee on Thermodynamics and Combustion
Polish Academy of Sciences

http://www.imp.gda.pl/archives-of-thermodynamics/

ARCHIVES OF THERMODYNAMICS

Experimental validation of a dynamic lumped parameter model of an automotive cabin

Ramon de Paoli Mendes[a], Juan José Garcia Pabon[b], Willian Moreira Duarte[a], Luiz Machado[a]

[a]Federal University of Minas Gerais, Av. Pres. Antônio Carlos, Belo Horizonte/MG 31270-901, Brazil
[b]Federal University of Itajubá, Av.. BPS, Itajubá/MG 37500 903, Brazil
*Corresponding author email: ramondepaoli@yahoo.com.br

Received: 12.06.2023; revised: 09.10.2023; accepted: 06.12.2023

Abstract

The objective of this work is to propose a thermal model for predicting the average air temperature inside the passenger cabin of a small-sized car that uses an HVAC system. The adopted model is a lumped parameter model that accounts for nine heat sources acting on the cabin. Additionally, the model presents a methodology for calculating the temperature at the evaporator outlet considering a linear temperature drop between its inlet and outlet as a function of sensitive heat, latent heat, evaporator input temperature, absolute humidity, enthalpy and specific heat. Sixteen experimental tests were conducted on a commercial vehicle under various operating conditions to validate the presented model. The maximum average relative deviation between the experimental and theoretical results was 17.73%.

Keywords: Thermal model; Automotive cabin; HVAC

Vol. 45(2024), No. 1, 119–128; doi: 10.24425/ather.2024.150444

Cite this manuscript as: de Paoli Mendes, R., Garcia Pabon, J.J., Moreira Duarte, W., & Machado, L. (2024). Experimental validation of a dynamic lumped parameter model of an automotive cabin. *Archives of Thermodynamics* 45(1), 119–128.

1. Introduction

The temperature control in the automotive cabin constitutes the main objective of the vehicle's HVAC system. The search for thermal comfort increases the consumption of the air conditioning system and consequently the fuel consumption. The use of air conditioning leads to an increase in total fuel consumption of 23 to 41% [1]. Additionally, in the United States alone, before 2004 around 26 billion liters of fuel were used annually, to ensure passenger thermal comfort [2].

Some of the most commonly used criteria for evaluating thermal comfort, such as the predicted mean vote (PMV) and the percentage of dissatisfied people (PPD), use the thermal energy stored in the human body and individual metabolic rate as a reference for evaluation [3,4]. The PMV and PPD equations can be found in ISO 7730 standard [5]. Both PMV and PPD depend on the cabin temperature, which is why it is necessary to understand how the cabin temperature varies.

In this sense, Shimizu et al. [6] investigated the transient thermal loads acting on the automotive cabin. In their article, they showed that in the air conditioning recirculation mode, the main thermal load is radiation, accounting for about 50% of the total. However, when air renewal is enabled, the main thermal

Nomenclature

A – area, m^2
B – extinction coefficient
C – specific heat at constant pressure, J/ (kg K)
C – solar radiation factor
h – enthalpy, J/kg
H – heat exchange coefficient, W/(m^2 K)
$\dot{I}$ – solar irradiance, W/m^2
k – thermal conductivity, W/ (m K)
m – mass, kg
$\dot{m}$ – mass flow rate, kg/s
n – rotation speed, rpm
N – number
P – pressure, Pa
$\dot{Q}$ – thermal load, W
T – temperature, ^{o}C
U – overall heat transfer coefficient, W/(m^2 K)
Y – radiation ratio
V – speed, km/h

Greek symbols

α – angle with the horizontal, rad
β – solar angle, rad
ϕ – relative humidity [%]
λ – plate thickness, m
θ – angle of solar incidence, rad
ρ – reflectivity coefficient
τ – transmissivity
ω – absolute humidity

Subscripts and Superscripts

amb – environmental
ap – apparent
air – air
atm – atmospheric
c – clarity
cab – cabin
dif – diffuse solar radiation
dir – direct solar radiation
e – external
eev – evaporator inlet
exa – exhaustion
$hvac$ – air conditioning system
i – internal
ind – indirect solar radiation
lat – latent
lv – steaming
met – metabolic
mot – engine
p – people
ref – reflected solar radiation
ren – renovation
rec – recirculation
s – saturation
sev – evaporator output
sen – sensitive
$vent$ –ventilation
w – water
z – Zenith

Abbreviations and Acronyms

MARD– Mean Absolute Relative Deviation
PMV – predicted mean vote
PPD – percentage of dissatisfied people

load to be countered is the ventilation thermal load, corresponding to about 50% of the total. Michalek et al. [7] considered the energy balance in the automotive cabin as the sum of metabolic loads, loads that pass through the windows, and loads inside the vehicle, such as infiltration and engine loads. In their work, the energy balance was written considering the average temperature of the automotive cabin, and the comparison of the dynamic model with experimental results obtained good proximity. Khayyam et al. [8] described in their work the modeling of the automotive cabin as a function of the thermal loads acting on it. In their work, they considered the metabolic thermal loads, direct solar radiation, diffuse solar radiation, reflected solar radiation, environmental radiation, exhaust system load, motor load, ventilation load, and HVAC load. Jha et al. [9] proposed in their model that the main thermal loads are solar radiation, infiltration thermal load, fan motor thermal load, internal combustion engine thermal load, floor load, and metabolic thermal load. The method used by Jha et al. [9], as well as by Khayyam et al. [8] to calculate solar radiation is presented in the ASHRAE handbook [10]. In the study of Khayyam et al. [8], the model is used in conjunction with an energy management system achieving a 47% reduction in energy consumption. In the research presented by Jha et al. [9], the model is validated in a wind tunnel and steady-state conditions, with the largest difference between predictions and experimental results being 15%.

Marcos et al. [11] calculated the metabolic thermal load using the ISO 7730 standard. The window thermal load was determined by adding the thermal loads that entered through convection due to the temperature difference between the glass and the cabin air. The authors found the temperature of the glass by performing thermodynamic balance on it, considering a steady state. In their model, the authors considered that the energy fraction that enters through the opaque lateral and rear parts of the vehicle is negligible compared to the thermal load that enters through the windows. They validated the presented model using experimental data measured in a BMW series 1 with different types of occupancy and speed, and the largest difference between experimental results and simulations was 4.6°C. Torregrosa-Jaime et al. [12] presented a similar work, where they developed and validated a thermal model for an ALTRA Daily electric van.

Fayazbakhsh and Bahrami [13] described a transient thermal model of the automotive cabin, similar to the one presented by Khayyam et al. [8]. They calculated the direct, diffuse, and reflected incident radiation using the method proposed by ASHRAE [10] and determined the enthalpies of humid air using the equations presented by Wilhelm [14]. Their work showed that the thermal loads from reflected radiation, the engine, and the exhaust were negligible, while the thermal loads from direct radiation and ventilation had the most significant impact on the total thermal load of the cabin.

Lee et al. [15] proposed a transient model to predict the internal temperature of a car cabin. The model assumed that the air properties inside the cabin are spatially uniform, the thermal load of passengers is 158 W per person, heat exchange by radiation between internal components of the cabin is negligible, the heat transfer coefficient between the cabin and the environment is calculated as a function of vehicle speed, and thermal loads from the floor and trunk are negligible. The authors also considered that the transmissivity and absorptivity properties are dependent on the angle of incidence of the radiation and modeled these properties according to the ASHRAE [16]. They validated the model in a climate chamber with a roller dynamometer, and the deviation between the model results was 5%. Finally, the authors used the model to simulate modifications in the vapor compression cycle and compared the performance of the air conditioning system operating with the refrigerants R134a, R152a, R444A, R445A, and R1234yf, with the latter being the best-performing fluid. Selow et al. [17] presented a similar work, including a model of the car cabin in the air conditioning system, but they used an empirical model for the car cabin.

Due to new vehicle technologies such as electric or hybrid cars, it becomes necessary to understand how the various systems that compose them affect the consumption of electrical energy by the vehicle and how this impacts the used battery. In this sense, the works of Ramsey et al. [18], and Liu and Zhang [19] address the thermal modeling of the automotive cabin, focusing on how the HVAC system impacts the vehicle's energy consumption. For larger vehicles, the same thermal loads act upon them. However, considering the properties of air as homogeneous throughout the entire vehicle is not possible. In this regard, Delgado et al. [20] studied the thermal modeling of a bus and obtained results for separate regions between passengers and the driver.

As regards the finite volume technique, it has a relatively high computational cost compared to the concentrated parameter model used in the aforementioned works. There are many studies using the finite volume simulation approach [21–23]. The use of finite volume techniques for thermal modeling of environments in many situations is due to the lack of knowledge of the equations that model a given process. For example, a thermal model of the automotive cabin that considers the inflow temperature through the HVAC system analytically was found only in Ramsey´s work [18] and it utilizes the entropy information at the inlet and outlet of the evaporator to calculate the evaporator's outlet temperature.

Therefore, this study not only thermally models the cabin but also adds a methodology for calculating the inflow air temperature in the cabin, as a function of sensitive heat, latent heat, evaporator input temperature, absolute humidity, enthalpy, and specific heat. This approach allows the modeling of the temperature at the evaporator outlet considering a linear drop with its inlet. It serves as a temperature estimate for the calculation of the refrigerating thermal load. In the following chapter, the thermal model is presented, followed by a description of the apparatus and experimental conditions used for comparative analysis with experimental data. Next, the results are evaluated and discussed, and finally, the conclusions are drawn.

2. Thermal model

Geometrically, the automotive cabin was modeled in 10 parts: front panel and glass, right and left side panels, right and left side glass, roof, floor, rear panel, and rear glass. Figure 1 presents the modeling of the car separated into opaque and translucent parts. The car parts were used in the thermal load calculations and the individual areas are represented in Table 1.

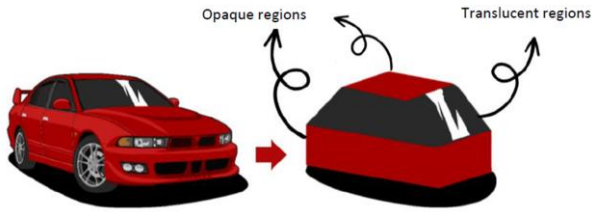

Fig. 1. Automotive cabin regions.

To quantify the thermal loads inside the cabin, knowledge of the dimensions of each region and, also, of the properties of the materials is necessary. Table 1 shows the area, surface inclination relative to the horizontal, and transmissivity of the glass, which were obtained based on the SpaceFox vehicle used in the model validation.

Table 1. Geometric model information.

Surface	Area [m²]	Inclination [deg]	Transmissivity
Front glass	0.936	30	0.78
Left side glass	0.7339	80	0.36
Right side glass	0.7339	80	0.36
Rear window	0.576	30	0.78
Roof	3.6	–	–
Right panel	3.26	–	–
Left panel	3.26	–	–
Front panel	0.66	–	–
Floor	3.6	–	–
Rear panel	0.66	–	–

This model considers 9 types of thermal loads acting on the cabin. These include the metabolic thermal load ($\dot{Q}_{met}$), direct solar radiation thermal load ($\dot{Q}_{dir}$), diffuse solar radiation thermal load ($\dot{Q}_{dif}$), reflected solar radiation thermal load ($\dot{Q}_{ref}$), internal combustion engine thermal load ($\dot{Q}_{mot}$), exhaust system thermal load ($\dot{Q}_{exa}$), environmental thermal load ($\dot{Q}_{amb}$), ventilation thermal load ($\dot{Q}_{vent}$), and HVAC system thermal load ($\dot{Q}_{hvac}$). The variation of the cabin's average temperature (T_{cab}) over time can be calculated as a function of the sum of the thermal loads entering the cabin:

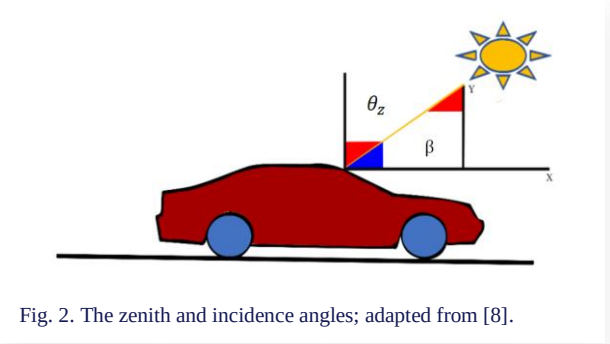

Fig. 2. The zenith and incidence angles; adapted from [8].

$$m_{cab} \cdot c \cdot \frac{dT_{cab}}{dt} = \dot{Q}_{met} + \dot{Q}_{dir} + \dot{Q}_{dif} + \dot{Q}_{ref} + \dot{Q}_{amb} + \dot{Q}_{exa} + \dot{Q}_{mot} + \dot{Q}_{vent} - \dot{Q}_{hvac}, \quad (1)$$

where m_{cab} represents the total mass of the cabin and c denotes its specific heat. However, the temperature of the solid elements inside the cabin differs from the average air temperature. The mass of the solid elements in the cabin and the thermal properties of the materials allow separate balancing of the heating (or cooling) of these elements over time and the calculation of their temperature change, and thus the accumulated heat.

The main simplifications made in the developed model are:

- The cabin mass (m_{cab}) is the sum of the air mass and the mass of seats.
- The specific heat capacity of the cabin (c) is the average between the specific heat capacity of the air and that of the seats.
- The energy exchanged through radiation and convection between the internal components of the cabin, air, and seats is negligible.
- Relative humidity at the evaporator outlet is equal to 0.9.

The calculation results were compared with experimental data.

2.1. Metabolic thermal load

The metabolic thermal load is the thermal load originating from the passengers occupying the automotive cabin. It can be determined based on the height and weight of the occupants as mentioned by Fayazbakhsh and Bahrami [13], but the value per person is around 100 W [10] and this value is adopted in the present model. The total metabolic thermal load is given by:

$$\dot{Q}_{met} = N_p \cdot 100, \quad (2)$$

where N_p represents the number of occupants in the cabin.

2.2. Direct solar radiation thermal load

The direct solar radiation thermal load ($\dot{Q}_{dir}$) is expressed as:

$$\dot{Q}_{dir} = \sum(\dot{I}_{dir} \cdot \tau \cdot A), \quad (3)$$

where A denotes the surface area of the car part described in Table 1, and $\dot{I}_{dir}$ is the direct solar irradiance. The portion of the radiation transmitted to the cabin must take into account the transmissivity (τ) of the material. The transmissivity of the glass was determined according to the instructions provided in the ASHRAE handbook [16], and its methodology has been evaluated in the work of Lee et al. [15]. The direct solar irradiance is calculated based on the apparent solar irradiation ($\dot{I}_{ap}$), the extinction coefficient (B), the zenith angle (θ_z), and the solar angle (β), according to the equation:

$$\dot{I}_{dir} = \dot{I}_{ap} \cdot N_c \cdot e^{(-B \cdot \mathrm{sen}(\beta))}, \quad (4)$$

where β is the solar elevation angle (Fig. 2) measured between the sun's rays and the horizontal at the point of incidence and N_c represents the clarity number. Parameter $\mathrm{sen}(\beta)$ allows the calculation of $\dot{I}_{dir}$ to vary depending on the position of the sun in relation to the angle of incidence. The zenith angle (θ_z) is the angle between the sun's rays and the normal to the surface (Fig. 2). The extinction coefficient (B) and the apparent solar radiation ($\dot{I}_{ap}$) were determined according to ASHRAE [10] for all months of the year 1964 in the USA. The value of the extinction coefficient was researched by Horvath [24] and in this work, a value of 0.15 is considered. The value of apparent solar radiation ($\dot{I}_{ap}$) accepted varies from 1367 W/m² to 1413 W/m² [25]. In this study, a value of 1413 W/m² is used. The clarity number (N_c) was determined in the ASHRAE handbook [26], and it is reasonable to consider it equal to 1.

2.3. Diffused solar radiation thermal load

Diffuse solar radiation is part of the radiation that indirectly strikes the surface of the automobile. It is calculated by multiplying the surface area by the indirect solar irradiance ($\dot{I}_{ind}$):

$$\dot{Q}_{dif} = \sum(\dot{I}_{ind} \cdot \tau \cdot A). \quad (5)$$

Diffuse solar radiation can be broken down into components that strike vertical and non-vertical surfaces. For vertical surfaces, it is necessary to calculate the ratio (Y) of the diffuse sky radiation to the surface radiation [10]:

$$Y = 0.55 + 0.437\cos(\theta_z) + 0.313\cos^2(\theta_z), \quad \text{for } \cos(\theta_z) > -0.2,$$

$$Y = 0.45\alpha, \quad \text{for } \cos(\theta_z) \leq -0.2.$$

Further, $\dot{I}_{ind}$ depends on the solar radiation factor (C) and the angle the surface makes with the horizontal (α). This yields for vertical surfaces:

$$\dot{I}_{ind} = C \cdot Y \cdot \dot{I}_{dir}, \tag{6}$$

and for other surfaces:

$$\dot{I}_{ind} = C \cdot \dot{I}_{dir} \cdot \frac{(1+\cos(\alpha))}{2}. \tag{7}$$

2.4. Reflected solar radiation thermal load

Reflected solar radiation is part of the radiation that strikes the surface of the automobile after being reflected by clouds, the ground, and the surrounding objects and may be expressed as:

$$\dot{Q}_{ref} = \sum(\dot{I}_{ref} \cdot \tau \cdot A), \tag{8}$$

where $\dot{I}_{ref}$ denotes the reflected solar irradiance, which depends on the direct solar irradiance and the ground reflectivity coefficient (ρ):

$$\dot{I}_{ref} = \dot{I}_{dir} \cdot (C + \sin(\beta)) \cdot \rho \cdot \frac{(1-\cos(\alpha))}{2}. \tag{9}$$

The reflectivity coefficient ρ can be considered equal to 0.28 second ASHRAE [10]. Parameter C can be determined according to Table 7 of Chapter 30 of ASHRAE [10].

2.5. Environmental thermal load

The environmental thermal load is calculated based on the temperature difference between the cabin air (T_{cab}) and the ambient air (T_{amb}):

$$\dot{Q}_{amb} = \sum(A \cdot U \cdot (T_{amb} - T_{cab})), \tag{10}$$

where U is the overall heat transfer coefficient, calculated as the inverse of thermal resistance. It considers the heat transfer coefficient by convection of the internal cabin air (H_i), the heat transfer coefficient of the external cabin air (H_e), the thermal conductivity of the surface (k), and its thickness (λ). The external heat transfer coefficient by convection can be determined from [27]:

$$H_e = 1.163 \cdot (4 + 12 \cdot V^{0.5}), \tag{11}$$

where V represents the air velocity if the vehicle is stationary, or the speed of the automobile if it is in motion. The internal heat transfer coefficient can be calculated considering natural convection inside the automotive cabin [28]. According to Creder [29], considering stationary air, the heat transfer coefficient varies from 8.29 to 9.26 W/(m² K). In the present study, an average value of 8.77 W/(m² K) is considered.

2.6. Exhaust thermal load

Due to the temperature difference between the motor exhaust gases and the cabin, part of the energy is transferred to the cabin through the floor. Thus:

$$\dot{Q}_{exa} = A_{exa} \cdot U_{exa} \cdot (T_{exa} - T_{cab}). \tag{12}$$

In the equation above, A_{exa} is the contact area between the cabin surface and the automobile exhaust pipe. The overall heat transfer coefficient U_{exa} can be calculated as the inverse of the thermal resistance between the exhaust pipe surface and the automobile cabin. The internal heat transfer coefficient to the cabin is calculated as described with regard to the calculation of the ambient thermal load (Eq. (10)). Finally, the temperature of the exhaust gases can be estimated as [8]:

$$T_{exa} = 0.138 \cdot n + 63, \tag{13}$$

where n is the car engine's angular speed.

2.7. Internal combustion engine thermal load

The internal combustion engine reaches high temperatures, and as a result, heat transfer occurs to the cabin through the front surface (A_{mot}). The resulting thermal load is expressed by:

$$\dot{Q}_{mot} = A_{mot} \cdot U_{mot} \cdot (T_{mot} - T_{cab}), \tag{14}$$

where U_{mot} represents the heat transfer coefficient from the engine, which can be determined as the inverse of the thermal resistance between the engine and the automotive cabin. The temperature of the engine (T_{mot}) can be estimated as a function of its rotation speed [8]:

$$T_{mot} = -2 \cdot 10^{-6} \cdot n^2 + 0.0355 \cdot n + 77.5. \tag{15}$$

2.8. Ventilation thermal load

When breathing, passengers release CO_2 inside the cabin, therefore air renewal is required. There are different percentages of air renewal relative to the total air mass of the cabin for different automotive vehicles. A minimum of 13% of fresh air relative to the total cabin volume for one passenger and 48% of fresh air for four passengers is recommended [30].

The ventilation thermal load can be calculated as a function of the mass flow rate of ventilation air ($\dot{m}_{air}$) - a mixture of the mass flow rate of fresh air and recirculated air - and the difference in enthalpy between the air at ambient temperature (h_{amb}) and the air at cabin temperature (h_{cab}):

$$\dot{Q}_{vent} = \dot{m}_{air} \cdot (h_{amb} - h_{cab}). \tag{16}$$

The enthalpy of the air in the cabin and also in the environment can be determined based on the temperature (T) and humidity ratio (ω) [13]:

$$h = (1.006 \cdot T + (2501 + 1.770 \cdot T) \cdot \omega) \cdot 10^3, \tag{17}$$

$$\omega = 0.62198 \cdot \frac{\phi \cdot P_s}{P - \phi \cdot P_s}, \tag{18}$$

where P_s is a saturation vapor pressure, P is a pressure and ϕ is a relative humidity. The thermal load of ventilation carries both the latent heat and sensible heat components. The enthalpy of water vapor at temperature T can be evaluated according to Wilhelm [31]:

$$h_w = (2502 + 1.775 \cdot T) \cdot 10^3. \tag{19}$$

Knowing the enthalpies of water vapor at a given environment temperature $(h_{w,amb})$ and the cabin temperature $(h_{w,cab})$, and the mass flow rate of fresh air $(\dot{m}_{ren})$, it is possible to calculate the latent heat and sensible heat that enters the cabin, respectively:

$$\dot{Q}_{lat} = \dot{m}_{ren} \cdot (h_{w,amb} - h_{w,cab}), \quad (20)$$

$$\dot{Q}_{sen} = \dot{Q}_{vent} - \dot{Q}_{lat}. \quad (21)$$

2.9. HVAC thermal load

The evaporator is responsible for discharging the total thermal load coming from the different sources previously mentioned. The heat removed by the evaporator ($\dot{Q}_{hvac}$) can be calculated by considering the mass flow rate of air that passes through it $(\dot{m}_{air})$, the specific heat of the air (c_{air}), and the temperature difference of the air between the inlet (T_{eev}) and outlet (T_{sev}):

$$\dot{Q}_{hvac} = \dot{m}_{air} \cdot c_{air} \cdot (T_{eev} - T_{sev}). \quad (22)$$

The ambient temperature entering the evaporator is the weighted average of the fresh air $(\dot{m}_{ren})$ and recirculated air mass flow rates $(\dot{m}_{rec})$. Therefore:

$$T_{eev} = \frac{(\dot{m}_{ren} \cdot T_{amb} + \dot{m}_{rec} \cdot T_{cab})}{\dot{m}_{air}}. \quad (23)$$

The absolute humidity entering the evaporator can be calculated as a weighted average between the fresh air and recirculated air mass flow rates:

$$\omega_{eev} = \frac{(\dot{m}_{ren} \cdot \omega_{amb} + \dot{m}_{rec} \cdot \omega_{cab})}{\dot{m}_{air}}. \quad (24)$$

Figure 3 shows the schematic representation of the integration of the evaporator, the evaporator fan, and the air inlet and outlet.

To calculate the evaporator outlet temperature and humidity, an energy balance is considered. Combining Eqs. (21), (22), and (24) the following is obtained:

$$T_{sev} = T_{eev} - h_{lv}\left(\frac{(\dot{m}_{ren}\omega_{amb} + \dot{m}_{rec}\omega_{cab})}{\dot{m}e_{air}} - \omega_{sev}\right)\frac{\dot{Q}_{sen}}{c_{air} \cdot \dot{Q}_{lat}}. \quad (25)$$

In this model, the relative humidity at the evaporator outlet (ϕ_{sev}) is considered to be 0.9, and the absolute humidity in the cabin to be the weighted average between the ambient absolute humidity and the one supplied by the evaporator. The evaporator and cabin outlet humidities are given by, respectively:

$$\omega_{sev} = 0.622 \cdot \frac{P_v}{P_{atm} - P_v}, \quad (26)$$

$$\omega_{cab} = \frac{(\omega_{sev} \cdot (\dot{m}_{ren} + \dot{m}_{rec}) + \omega_{amb} \cdot \dot{m}_{ren})}{\dot{m}_{ren} + \dot{m}_{rec}}, \quad (27)$$

where P_v is the vapor pressure and P_{atm} is the atmospheric pressure. The saturation vapor pressure of water, $P_{v,s}$, can be calculated using the classical Antoine equation [32]:

$$P_{v,s} = 133.3 \cdot 10^{8.07131 - \frac{1730.63}{(T + 233.426)}}. \quad (28)$$

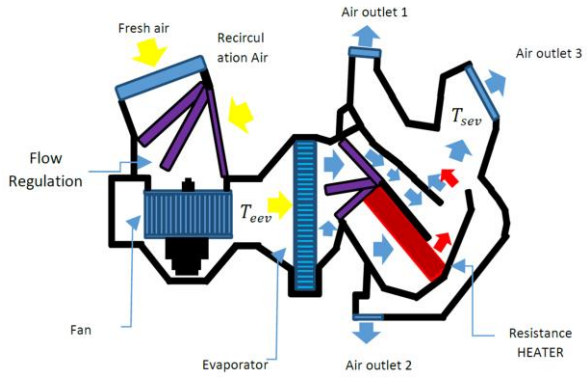

Fig. 3. Evaporator air distribution box.

The relative humidity can be calculated as the ratio between the vapor pressure and the saturation vapor pressure. Therefore:

$$P_v = \phi_{sev} \cdot P_{v,s}. \quad (29)$$

3. Experimentation

The tested vehicle was the 2013 white Volkswagen SpaceFox. It has a motor power of up to 101 horsepower (1.6 l) at 5250 rpm, 4 cylinders with a displacement of 1598 cm^3 and a compression ratio of 12.1:1. Figure 4 shows a photograph of the vehicle along with installed thermocouples and the notebook connected to the data acquisition board.

Sixteen T-type thermocouples with an uncertainty of 0.5ºC were used to measure the temperature at various points inside the automotive cabin for sixteen operating conditions. The National Instruments 9213 board was used for data acquisition, communicating with LabView software to read the thermocouples. Two thermocouples were positioned on the front glass, two on the rear glass, two on the left and right-side glasses, two on the ceiling, two on the floor, one at the air diffuser outlet, two in the cabin interior, and one outside the car recording the ambient temperature.

The thermocouples located inside the cabin were taken as a reference so that the average values between the two could be compared to the temperature predicted by the thermal model. The other thermocouples installed in different regions of the cabin were used to determine which surfaces undergo greater heating compared to the average of the internal thermocouples.

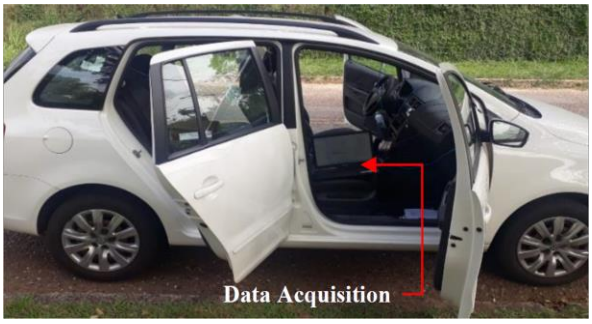

Fig. 4. Experimental vehicle.

The air velocity of the inflow was measured using an anemometer with an uncertainty of ± 0.3 m/s. Subsequently, the values were multiplied by the cross-sectional area of the evaporator (0.057375 m²) and by the density of the air, resulting in the mass inflow rates for the cabin. The expanded uncertainty calculation for the mass flow rate resulted in 0.0209 kg/s. The inflow mass rate values ($\dot{m}_{air}$) are presented in Table 2.

The vehicle was tested when stationary and while moving at a speed of 20 km/h. During the operation, two people were inside the vehicle, one being the driver and the other responsible for data acquisition. Both occupants of the vehicle were seated in the front seats. The fan controller was operated in 4 positions, each corresponding to different evaporator fan speeds and consequently different airflows. In all experiments, the pre-heater was not used, so that the temperature of the evaporator outlet was practically the same as that insufflated into the cabin. The air was blown towards the passengers from the front. The recirculation mode was also tested for each fan speed position.

The experiments were divided into two different days. On day 290 of 2022 (October 17), the experiments with the stationary vehicle were conducted. On day 291 of 2022 (October 18), the experiment was carried out with the vehicle moving at a speed of 20 km/h. For both days, the local relative humidity was 60%. The remaining experimental data, such as the time of the experiment, insufflated air flow rate, initial ambient temperature, initial cabin temperature, and engine rotation, are recorded in Table 2.

4. Results

The data obtained from simulation and experimentation are compared. In addition, the Pearson correlation coefficient (r) and the Mean Absolute Relative Deviation (MARD) are presented, respectively:

$$r = \frac{\Sigma\left(\left(T_{sim}-T_{sim_{mean}}\right)\cdot\left(T_{exp}-T_{exp_{mean}}\right)\right)}{\sqrt{\Sigma\left(\left(T_{sim}-T_{sim_{mean}}\right)^2\cdot\left(T_{exp}-T_{exp_{mean}}\right)^2\right)}}, \tag{30}$$

$$\mathrm{MARD} = \frac{1}{N}\cdot\sum\left|\frac{T_{sim}(i)-T_{exp}(i)}{T_{exp}(i)}\right|, \tag{31}$$

where the subscripts *sim* and *exp* refer to simulated and measured values, respectively, and mean represents the mean difference. Parameter *i* denotes a data point number, and *N* is the total number of the data set points.

The Pearson coefficient *r* varies from –1 to 1, indicating the strength and direction of the correlation between the variables. A value close to 1 indicates a strong positive correlation, meaning that when one variable increases, the other also increases. A value close to –1 indicates a strong negative correlation, meaning that when one variable increases, the other decreases. A value close to 0 indicates a weak or absent correlation between the variables. The MARD parameter is used to evaluate the accuracy of a model or simulation, focusing on the absolute mean difference between the data.

Regarding the comparison between experimental data and simulation, the Pearson correlation coefficient remained in the range between 0.79 and 0.99. The mean absolute relative deviation (MARD) between the experimental data reached its maximum of 17.73% (experiment 8), and its minimum of 1.05% (experiment 1), as can be observed from the results shown in Table 3.

Table 2. Experimental conditions.

Exp.	Day	Hour	T_{cab} [°C]	V [km/h]	$\dot{m}_{air}$ [kg/s]	$\dot{m}_{ren}$ [%]	T_{amb} [°C]	ϕ	n [rpm]
1	290	13:37-13:47	25.2	0	0.154	26	26.0	0.6	1000
2	290	13:59-14:09	23.0	0	0.223	26	25.0	0.6	1000
3	290	14:17-14:27	24.3	0	0.305	26	27.2	0.6	1000
4	290	14:49-14:59	23.2	0	0.389	26	28.8	0.6	1000
5	290	15:09-15:19	23.9	0	0.154	15	25.8	0.6	1000
6	290	15:27-15:37	24.5	0	0.223	10	24.8	0.6	1000
7	290	15:45-15:55	25.2	0	0.305	7	28.2	0.6	1000
8	290	16:01-16:11	25,0	0	0.389	6	26.7	0.6	1000
9	291	13:14-13:24	24.6	20	0.154	26	24.7	0.6	1500
10	291	13:32-13:42	26.9	20	0.223	26	26.5	0.6	1500
11	291	13:52-14:02	25.2	20	0.305	26	25.0	0.6	1500
12	291	14:14-14:24	25.0	20	0.389	26	26.6	0.6	1500
13	291	14:33-14:43	25.5	20	0.154	15	25.3	0.6	1500
14	291	14:53-15:03	26.0	20	0.223	10	26.1	0.6	1500
15	291	15:15-15:25	26.0	20	0.305	7	28.4	0.6	1500
16	291	15:40-15:50	25.8	20	0.389	6	24.5	0.6	1500

Table 3. MARD and Pearson coefficient.

Exp.	Pearson coeff. [%]	MARD [%]
1	99.20	1.05
2	99.21	2.15
3	98.81	4.83
4	90.77	2.71
5	96.03	10.05
6	97.07	7.90
7	98.40	12.60
8	96.79	17.73
9	93.85	6.05
10	81.51	4.12
11	87.78	4.18
12	79.29	5.96
13	95.93	6.68
14	95.16	5.44
15	94.35	7.63
16	81.66	3.65

The comparative graphs between the model and experimental data on the temperature inside the vehicle cabin are presented in Figs. 5–8. Figure 5 refers to the experiments of day 290 with indexes 1 to 4 in Table 3. In these experiments, the vehicle was stationary and exposed to the sun at the same time the HVAC system was activated. Four evaporator fan speeds were tested for the mixed air condition of fresh and recirculated air. Figure 6 also refers to the vehicle at rest and tested at four evaporator fan speed options, however, the air supplied was only the recirculated air with an additional amount of 0.02 kg/s [13] due to air infiltration into the vehicle - naturally, as the cabin due to air infiltration into the vehicle - naturally, as the cabin interior pressure is lower than the exterior pressure.

The vehicle was also tested at a speed of 20 km/h with four different fan speeds for the evaporator. Figure 7 refers to the test where the air supply was a mixture of fresh and recirculated air. Figure 8 shows the results for the case where the air supply was only recirculated air with an additional amount of 0.02 kg/s [13] due to natural air infiltration through the gaps in the cabin.

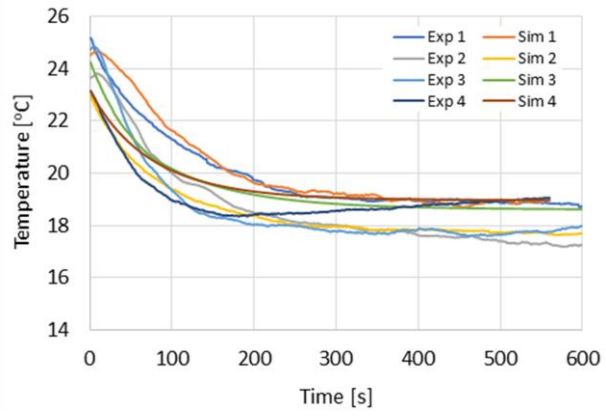

Fig. 5. Change of temperature of the vehicle cabin interior - comparison between model and experimental data: experiments 1 to 4.

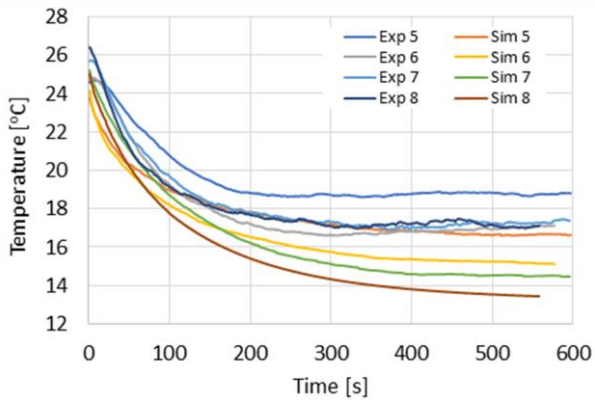

Fig. 6. Change of temperature of the vehicle cabin interior - comparison between model and experimental data: experiments 5 to 8.

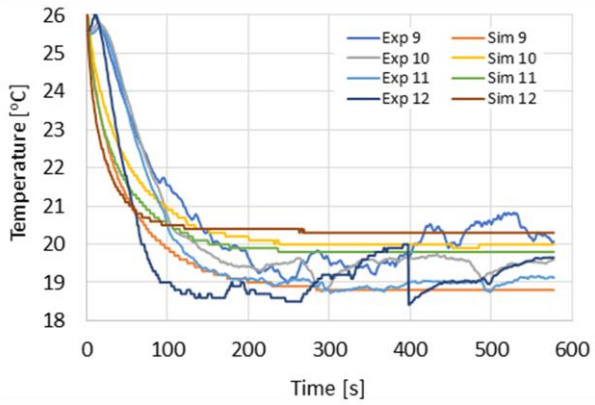

Fig. 7. Change of temperature of the vehicle cabin interior - comparison between model and experimental data: experiments 9 to 12.

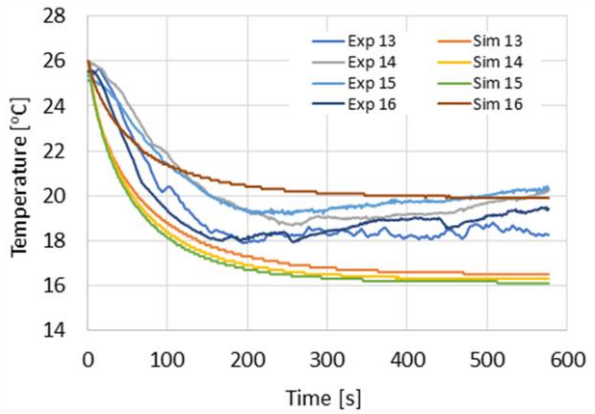

Fig. 8. Change of temperature of the vehicle cabin interior - comparison between model and experimental data: experiments 13 to 16.

As can be seen in the experimental data provided in Figs. 5–8, there is a slight increase in temperature initially after the HVAC is turned on before it starts to decrease. This occurs because the air being blown initially carries thermal energy stored due to the heating of the body and mechanical components of the system. The thermal model is unable to predict this

transient behavior for the initial few seconds of HVAC operation as it does not account for the energy stored in the stationary air within the ducts.

Regarding the transient regime, the time constant of the temperature curve slope is strongly influenced by the mass of the system being conditioned. In this sense, both the mass of the air and the mass of the seats interfere with how the thermal curve slope is constructed in the transient region. Determining the exact mass is a difficult task and varies considerably from vehicle to vehicle. In this work, the internal mass of the cabin was estimated to be 60 kg.

As regards the proposed formulation to calculate the temperature at the evaporator outlet (Eq. (25)), a linear temperature drop was considered based on physical parameters such as temperature, flow rate, pressure, and relative and absolute humidity. However, in real systems, the temperature drop between the inlet and outlet of the evaporator occurs parabolically with temperature curves very similar to the average temperature curves of the air inside the automotive cabin, as shown in the experimental results. This obviously indicates the strong relationship between the temperature of the supplied air and the average temperature of the automotive cabin.

The developed model can predict the thermal variation in the cabin more efficiently when the vehicle is at rest and in the air recirculation mode - as can be observed in Fig. 5. When the air renewal mode is activated and/or the vehicle is in motion, changes in the heat exchange coefficient with the environment interfere with the accuracy of the model.

Regarding the temperatures of the surfaces inside the automotive cabin, they are higher than the temperature of the air inside the cabin. Therefore, it is not possible to use them as a parameter to calculate the average temperature of the air inside the cabin. While the air temperature continues to drop from the start of the HVAC operation to the steady state, the surface temperatures increase and remain at a much higher level than the air temperature inside the cabin. As a result, the average of the temperatures provided by the surfaces or even the radiant temperature does not correspond to the average temperature of the air inside the cabin.

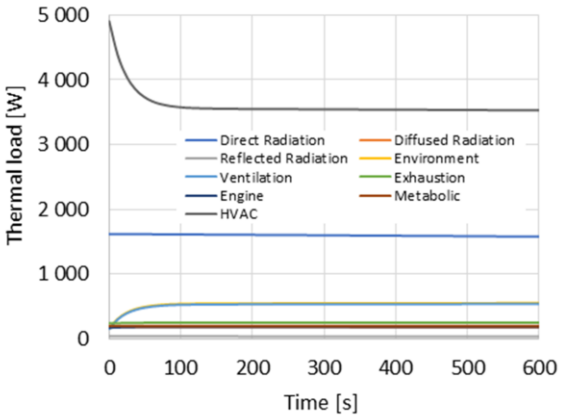

Fig. 9. Thermal loads for a stationary vehicle.

Figures 9 and 10 depict the nine thermal loads inside the cabin related to Eq. (1) for the stationary vehicle and the one moving at 20 km/h, respectively. For the simulation, the same mass flow rate of inflow air and the same percentage of fresh air were considered. It is observed that the car's motion modifies the heat exchange coefficient described by Eq. (11), increasing the percentage of environmental thermal load. The ventilation thermal load varied slightly when changing from 0 to 20 km/h, given that the low-speed variation did not account for changes in the mass flow rate of inflow air. The primary thermal load to be addressed by the HVAC system is the direct radiation thermal load.

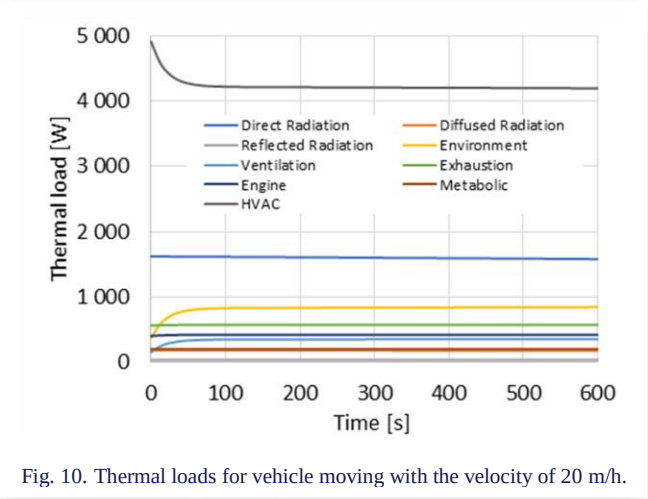

Fig. 10. Thermal loads for vehicle moving with the velocity of 20 m/h.

5. Conclusions

The thermal modeling of automotive cabins is difficult due to the different characteristics of each vehicle and, also, the environment in which it is located. Factors such as internal air mass, and the mass of seats and internal components of the cabin can alter the slope of the temperature curve during the transient period when compared to experimental data. In addition to this, the thicknesses of the bodywork, construction materials, and even the colors of the vehicles can alter the heat transfer coefficients and consequently bring uncertainties to the model. This justifies the trend found in the literature of many authors using modeling via finite volume technique.

Among the results, it was found that increasing the inflow rate and vehicle speed tends to decrease the model's suitability to the experimental data. However, even considering this, the model presented a maximum average relative deviation (MARD) of 17.73%. As for other studies found in the literature regarding thermal modeling of the automotive cabin, no proposal was found for calculating the temperature at the evaporator outlet. In this regard, most authors opted to directly measure this temperature using thermocouples.

Regarding thermal distribution in the cabin, it was noticed that surface temperatures cannot be used to determine the average air temperature inside it. Through experimental observations and simulation, it was found that the highest thermal load acting on the cabin is the direct radiation thermal load. These conclusions are in agreement with other research in the literature, such

as those presented in the works of Fayazbakhsh and Bahrami [13] and Khayyam et al. [8]. It is concluded that the thermal model proposed to determine the average temperature of the air inside the automotive cabin, when used, will present MARD below 20%. However, the characteristics of each vehicle - such as the air mass and seats - can significantly affect the transient state if not correctly determined.

Acknowledgement

This study was financed in part by the Coordenação de Aperfeiçoamento de Pessoal de Nível Superior – Brasil (CAPES) – Finance Code 001.

References

[1] Orofino, L., Amante, F., Mola, S., Rostagno, M., Villosio, G., & Piu, A. (2007). An integrated approach for air conditioning and electrical system impact on vehicle fuel consumption and performances analysis: DrivEM 1.0. *SAE Technical Paper Series*. doi: 10.4271/2007-01-0762

[2] Rugh, J.P., Hovland, V., & Andersen, S.O. (2004). Significant fuel savings and emission reductions by improving vehicle air conditioning. *15th Annual Earth Technologies Forum and Mobile Air Conditioning Summit*, April 13-15, Washington D.C. http://www.nrel.gov/vehiclesandfuels/ancillary_loads/pdfs/fuel_savings_ac.pdf [accessed 9 Oct. 2023].

[3] Moon, J. H., Lee, J. W., Jeong, C. H., & Lee, S. H. (2016). Thermal comfort analysis in a passenger compartment considering the solar radiation effect. *International Journal of Thermal Sciences*, 107, 77–88. doi: 10.1016/j.ijthermalsci. 2016.03.013

[4] Oh, M.S., Ahn, J.H., Kim, D.W., Jang, D.S., & Kim, Y. (2014). Thermal comfort and energy saving in a vehicle compartment using a localized air-conditioning system. *Applied Energy*, 133, 14–21. doi: 10.1016/j.apenergy.2014.07.089

[5] Ahilan, C., Kumanan, S., & Sivakumaran, N. (2010). Design and implementation of an intelligent controller for a split air conditioner with energy saving. *Advances in Modelling and Analysis C*, 65, 21–40.

[6] Shimizu, S., Hara, H., & Asakawa F. (1983). Analysis on air-conditioning heat load of a passenger vehicle. *International Journal of Vehicle Design*, 4(3), 292–311. doi: 10.1504/IJVD.1983.061317

[7] Michalek, D., Gehsat, C., Trapp, R., & Bertram, T. (2005). Hardware-in-the-loop-simulation of a vehicle climate controller with a combined HVAC and passenger compartment model. *IEEE/ASME (AIM) International Conference on Advanced Intelligent Mechatronics*, 24-28 July. 2, Monterey, USA, 1065–1070. doi: 10.1109/aim.2005.1511151

[8] Khayyam, H., Kouzani, A.Z., & Hu, E.J. (2009). Reducing energy consumption of vehicle air conditioning system by an energy management system. *IEEE Intelligent Vehicles Symposium*, 3-5 June, Xi'an, China, 752–757. doi: 10.1109/IVS.2009.5164371

[9] Jha, K.K., Bhanot, V., & Ryali, V. (2013). A simple model for calculating vehicle thermal loads. *SAE Technical Paper*, 2013-01-0855. doi: 10.4271/2013-01-0855.

[10] ASHRAE (2001). *ASHRAE Fundamental Handbook*. Atlanta, p. 30.

[11] Marcos, D., Pino, F.J., Bordons, C., & Guerra, J.J. (2014). The development and validation of a thermal model for the cabin of a vehicle. *Applied Thermal Engineering*, 66, 646–656. doi: 10.1016/j.applthermaleng.2014.02.054

[12] Torregrosa-Jaime, B., Bjurling, F., Corberán, J.M., Di Sciullo, F., & Payá, J. (2015). Transient thermal model of a vehicle's cabin validated under variable ambient conditions. *Applied Thermal Engineering*, 75, 45–53. doi: 10.1016/j.applthermaleng. 2014.05.074

[13] Fayazbakhsh, M.A., & Bahrami, M. (2013). Comprehensive modeling of vehicle air conditioning loads using heat balance method. *SAE Technical Paper*, 2013-01-1507. doi: 10.4271/2013-01-1507

[14] Wilhelm, L. R. (1976). Numerical calculation of psychrometric properties in SI units. *Transactions of the ASABE*, 19(2). doi: 10.13031/2013.36019

[15] Lee, H., Hwang, Y., Song, I., & Jang, K. (2015). Transient thermal model of passenger car's cabin and implementation to saturation cycle with alternative working fluids. *Energy*, 90, 1859–1868. doi: 10.1016/j.energy.2015.07.016

[16] ASHRAE. (2013). *ASHRAE Handbook, Fundamentals*. [chapter 15].

[17] Selow, J., Wallis, M., Zoz, S., & Wiseman, M. (1997). Towards a virtual vehicle for thermal analysis. *SAE Technical Paper Series*. doi: 10.4271/971841

[18] Ramsey, D., Boulon, L., & Bouscayrol, A. (2021). Modeling of an EV air conditioning system for energetic studies in summer. IEEE Vehicle Power and Propulsion Conference (VPPC), 25-28 October, Gijon, Spain. doi: 10.1109/VPPC53923.2021.9699119

[19] Liu, Y., & Zhang, J. (2021). Electric vehicle battery thermal and cabin climate management based on model predictive control. J. Mech. Des. Trans. ASME, 143, 1–8. doi: 10.1115/1.4048816

[20] Delgado, M.L., Jiménez-Hornero, J.E., & Vázquez F. (2023). Design, implementation and validation of a hardware-in-the-loop test bench for heating systems in conventional coaches. *Applied Sciences*, 13(4), 2212. doi: 10.3390/app13042212

[21] Paulke, S., & Ellinger, M. (2007). Air conditioning cabin simulation with local comfort rating of passengers. *2nd European Workshop on Mobile Air Conditioning and Auxiliary Systems – ATA / CRF*, 29-30 November, Torino, Italy.

[22] Singh, S., & Abbassi, H. (2018). 1D/3D transient HVAC thermal modeling of an off-highway machinery cabin using CFD-ANN hybrid method. *Applied Thermal Engineering*, 135, 406–417. doi: 10.1016/j.applthermaleng.2018.02.054

[23] Warey, A., Kaushik, S., Khalighi, B., Cruse, M., & Venkatesan, G. (2020). Data-driven prediction of vehicle cabin thermal comfort: using machine learning and high-fidelity simulation results. *International Journal of Heat and Mass Transfer*, 148, 119083. doi: 10.1016/j.ijheatmasstransfer.2019.119083

[24] Horvath, H. (1991). Spectral extinction coefficients of background aerosols in Europe, North and South America: A comparison. *Atmospheric Environment. Part A, General Topics*, 25, 725–732. doi: 10.1016/0960-1686(91)90071-E

[25] Iqbal, M. (1983). *An Introduction to Solar Radiation*. Academic Press Canada, Ontario. doi: 10.1111/jmp.12384

[26] ASHRAE. (1999). *Handbook Fundamentals*, SI. Atlanta.

[27] Wu, J., Jiang, F., Song, H., Liu, C., & Lu, B. (2017). Analysis and validation of transient thermal model for automobile cabin. *Applied Thermal Engineering*, 22, 91–102. doi: 10.1016/ j.applthermaleng.2017.03.084

[28] Tong, Z., & Liu, H. (2020). Modeling in-vehicle VOCs distribution from cabin interior surfaces under solar radiation. *Sustainability*, 12(14), 5526. doi:10.3390/su12145526

[29] Creder, H. (2004). INSTALAÇÕES DE AR CONDICIONADO. Livros Técnicos e Científicos Editora S.A. (LCT), Rio de Janeiro, 2004. [in Portuguese]

[30] Arndt, M., & Sauer, M. (2004). Spectroscopic carbon dioxide sensor for automotive applications. *Sensors 2004 IEEE*, 1, 24-27 October, Vienna, Austria, pp. 252–255. doi: 10.1109/icsens. 2004.1426149

[31] Singh, A.K., Singh, H., Singh, S.P., & Sawhney, R.L. (2002). Numerical calculation of psychrometric properties. *Building and Environment*, 37(4), 415–419. doi: 10.1016/S0360-1323(01) 00032-4

[32] Thomson, G.W.M. (1946). The Antoine equation for vapor-pressure. Data. *Chemical Reviews*, 38(1), 1–39. doi: 10.1021/cr60119a001